KSCE Journal of Civil Engineering (2024) 28(8):3176-3191
DOI 10.1007/s12205-024-1228-8

pISSN 1226-7988, eISSN 1976-3808
www.springer.com/12205

Geotechnical Engineering

Centrifuge Modeling of Soil Liquefaction Triggering: 2017 Pohang Earthquake

Dong-Hyeong Choi[a], **Tae-Hyuk Kwon**[b], **and Kil-Wan Ko**[c]

[a]*Dept. of Civil and Environmental Engineering, Korea Advanced Institute of Science and Technology (KAIST), Daejeon 34141, Korea*
[b]*Member, Dept. of Civil and Environmental Engineering, Korea Advanced Institute of Science and Technology (KAIST), Daejeon 34141, Korea*
[c]*Member, Dept. of Civil and Environmental Engineering, University of California, Davis, CA 95616, USA*

ARTICLE HISTORY

Received 20 June 2023
Revised 1st 28 December 2023
Revised 2nd 11 March 2024
Accepted 18 March 2024
Published Online 6 June 2024

KEYWORDS

Centrifuge modeling
Soil liquefaction
2017 Pohang earthquake

ABSTRACT

Soil liquefaction by earthquake results in significant soil deformation and can cause substantial damage to infrastructure. Accordingly, there is a critical need to analyze earthquake case histories, and such analysis should focus on elucidating ground motion characteristics and field measurement data associated with instances of soil. The most straightforward approach to identifying liquefaction triggering involves examining pore water pressure records, which is challenging in many susceptible areas due to the absence of installed pore water pressure transducers. Therefore, evaluating liquefaction commonly relies on surficial evidence, such as sand boil or lateral spreading. However, this evaluation can miss the liquefaction triggered case without such surficial evidence. This study modeled the 2017 Pohang liquefaction, a first-time occurrence in South Korea, through a centrifuge test replicating the liquefied site based on field investigations, including borehole tests and recorded earthquake motions. We comprehensively assessed liquefaction using the ratio of excess pore water pressure alongside analyses of acceleration time histories, shear stress-strain hysteresis, and time-frequency histories. These results were compared with a conventional method that overlooked pore water pressure, leading to overestimation. Furthermore, using a simplified method, we compared liquefaction triggering evaluation results from the centrifuge cone penetration test and on-site standard penetration test. This, along with the factor of safety, substantiated the validity of the centrifuge results.

1. Introduction

Earthquake case histories and the subsequent damages provide invaluable lessons to the engineering community on how to prepare for future seismic events. The Mexico City earthquake in 1985 (M_w 8.0) enlightened the importance of site amplification in soils (Mendoza and Auvinet, 1988). The 1995 Hyogo-Ken Nanbu earthquake (M_w 6.9) served as a pivotal event in seismic design, which shifted the focus from forced-based design to performance-based design (Inagaki et al., 1996; Soga, 1998). Accordingly, an assessment and reconnaissance of the case histories are necessary to connect the past catastrophe with future advancements in seismic design.

The excess pore water pressure buildup during rapid cyclic loading the effective stress of soil which leads to soil liquefaction, predominantly observed in saturated loose sandy soil. This phenomenon gained significant attention following the Niigata earthquake in 1964. Notably, the collapse of the Kawagishicho apartment building, despite minimal structural damage, spurred investigations into the relationship between liquefaction and structural integrity (Seed and Idriss, 1967). Furthermore, the 1964 earthquake in Alaska provided insights into lateral spreading as a prominent indicator of liquefaction, given the observed damage resulting from this phenomenon (Youd and Bartlett, 1991).

When liquefaction is triggered, the soil exhibits pronounced nonlinearity in both stiffness and damping with increased shear strain levels. Given this complexity along with heterogeneity, while computational challenges such as extended processing times and accounting for soil nonlinearity are addressed, numerical

CORRESPONDENCE Kil-Wan Ko kilko@ucdavis.edu Dept. of Civil and Environmental Engineering, University of California, Davis, CA 95616, USA

constitutive models still necessitate experimental validation to ensure accuracy. Despite the experimental limitations (e.g., multiple layers with different soil types, varying layer thickness, irregular boundaries between layers, etc.), centrifuge tests are an effective viable alternative for obtaining measurements on behalf of the field measurement. This is accomplished by replicating in-situ stress conditions and simulating soil responses from small strains to failure, thereby serving as a substitute for field measurements. Many studies have utilized centrifuge tests to scrutinize damages from the field case histories (Dobry et al., 2013; EI-Sekelly et al., 2016) and seismic responses of buried pipelines, embankments, and structure-foundation systems (Ha et al., 2010; Bertalot et al., 2012; Tiznado et al., 2020).

To verify the initiation of liquefaction during the earthquake, the most direct and simple approach is to measure and evaluate pore water pressure records at sites. However, since pore water pressure sensors are rarely installed at the site, obtaining such records in many liquefaction-prone regions proves challenging. Typically, the assessment of liquefaction relies on surface manifestations, such as sand boil or lateral spreading, which are consequence of liquefaction. It is crucial to distinguish between the triggering and consequence of liquefaction. Even if liquefaction is triggered, the potential exists for no discernible surface manifestation, making damage unpredictable (Maurer et al., 2014; van Ballegooy et al., 2015a, 2015b; Hutabarat and Bray, 2021). To enhance the precision and cost-effectiveness of liquefaction mitigation, a comprehensive understanding of the triggering mechanisms is imperative.

On November 15, 2017, at 05:29 UTC, a seismic event with a magnitude M_w of 5.5 occurred approximately 7.5 km north of Pohang-si, Gyeongsangbuk-do (36.11°N, 129.37°E). This *2017 Pohang earthquake* is reported to have originated from a reverse fault strike movement at a depth ranging between 7 to 9 km within the Miocene Pohang Basin (KMA, 2018; MOIS, 2018). The economic impact of this event on society was approximately 13-fold greater than that of the 2016 Gyeongju earthquake in South Korea (KMA, 2017; MOIS, 2017). Notably, the triggering of soil liquefaction on November 15, 2017, marked the first instance since the inception of earthquake observations by the Korea Meteorological Administration (KMA) in 1978 (NDMI, 2019).

A previous case history study on liquefaction indicated an average earthquake magnitude (M_w) of 7.0 in instances where liquefaction has been triggered (Ilgaç, 2022). In contrast, despite its modest magnitude, the 2017 Pohang earthquake-triggered liquefaction, which is out of 1 sigma (M_w 6.1 – 7.9) from the average magnitude, presents a unique case globally with surface evidence. This anomaly underscores the necessity for an in-depth investigation into the triggering mechanisms of liquefaction.

The objective of this study is to replicate the triggering of the Pohang liquefaction phenomenon through a dynamic centrifuge experiment, scrutinizing the dynamic characteristics of liquefied soil and resultant ground deformation. The observation of liquefaction triggering incorporates analyses of the excess pore water pressure ratio (r_u) records, acceleration time histories, shear stress-strain responses, and time-frequency responses. Concurrently, the evaluation of ground deformation involves monitoring horizontal and vertical displacements of the ground surface, alongside assessing the suitability of previously proposed liquefaction evaluation methods for this distinctive case. Furthermore, the factor of safety for liquefaction (FS_{liq}) is assessed by comparing results from the field standard penetration test (SPT) and centrifuge cone penetration test (CPT) conducted.

2. Centrifuge Modeling

The experiment was conducted at the KOCED Geo-centrifuge center in KAIST, Daejeon, Korea. The equipment used in the experiment is an asymmetric beam-type centrifuge with a radius of 5 m and a maximum capacity of 240 g-ton. It can reproduce a centrifugal acceleration of 130 g-level for a maximum load of 1,300 kg (Kim et al., 2013a). In this study, the applied centrifugal acceleration was 30 g-level at the ground surface level. A self-balanced electro-hydraulic shaking table was used to apply the

Table 1. 2017 Pohang Earthquake Sites for Recorded Stations, Borehole Locations, and Locations of Soil Ejecta (NDMI, 2019)

Sites	Latitude	Longitude
Epicenter	36° 07' 12.00" N	129° 21' 36.00" E
Old port	36° 02' 44.70" N	129° 22' 36.40" E
CH-1	36° 07' 06.60" N	129° 21' 41.63" E
CH-2	36° 06' 58.48" N	129° 22' 01.08" E
CH-3	36° 06' 37.39" N	129° 18' 25.68" E
CH-4	36° 02' 32.79" N	129° 22' 26.74" E
CH-5	36° 01' 56.03" N	129° 22' 46.33" E
Locations of liquefaction occurrence observed by soil ejecta	36° 01' 36.20" N	129° 22' 38.24" E
	36° 01' 37.26" N	129° 22' 40.51" E
	36° 01' 34.66" N	129° 22' 41.61" E
	36° 01' 41.30" N	129° 22' 45.76" E
	36° 01' 51.45" N	129° 22' 53.20" E
	36° 01' 57.92" N	129° 22' 24.46" E
	36° 02' 06.52" N	129° 22' 30.01" E
	36° 02' 11.99" N	129° 22' 15.15" E
	36° 02' 11.38" N	129° 22' 16.28" E
	36° 02' 11.40" N	129° 22' 18.05" E
	36° 02' 10.96" N	129° 22' 18.28" E
	36° 02' 12.05" N	129° 22' 21.28" E
	36° 02' 14.21" N	129° 22' 21.51" E
	36° 02' 16.74" N	129° 22' 20.72" E
	36° 02' 18.68" N	129° 22' 21.59" E
	36° 02' 19.84" N	129° 22' 22.69" E
	36° 02' 31.48" N	129° 22' 25.99" E
	36° 01' 26.45" N	129° 22' 39.28" E
	36° 01' 40.40" N	129° 22' 25.76" E
	36° 06' 58.31" N	129° 22' 00.05" E

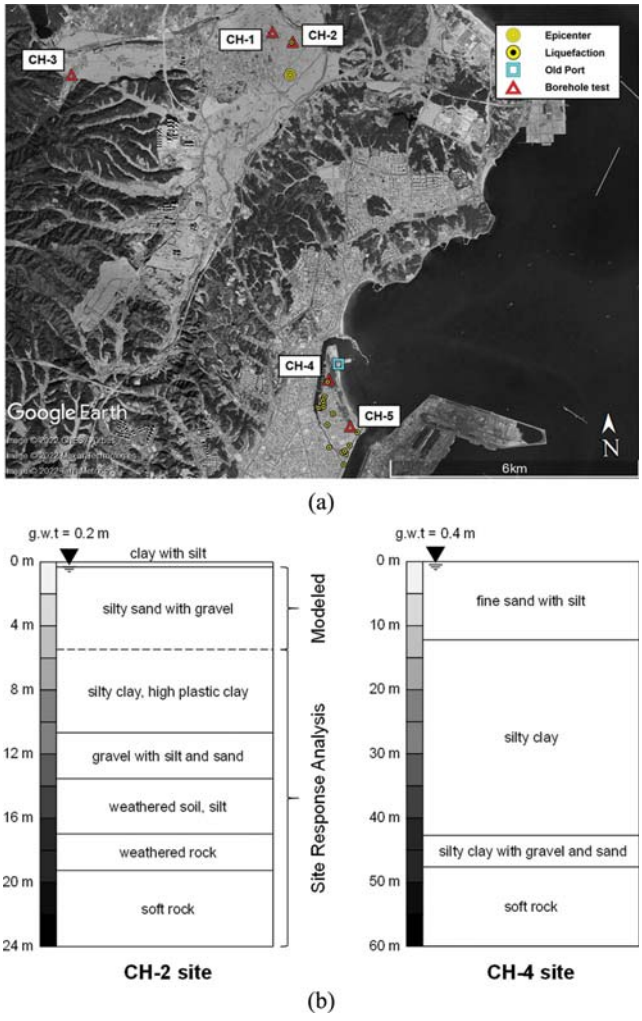

Fig. 1. Study Sites in City of Pohang: (a) Locations of Liquefaction Triggering with Borehole Test, (b) Borehole Test Results of Sites CH-2 and CH-4

input motion to the soil model. The maximum base acceleration was 20 g under the centrifugal acceleration of 30 g with a maximum payload of 700 kg. This corresponds to 0.67 g of seismic acceleration at the prototype scale. The earthquake simulator (shaking table) can excite a range of loading frequencies of 30 – 300 Hz for random vibration and 40 – 200 Hz for sinusoidal excitations, respectively (Kim et al., 2013b). In this study, the obtained test results and descriptions are expressed at a prototype scale by applying the scaling factor 30 (Madabhushi, 2017).

2.1 Target Field Site

A total of 20 sites observed sand boils during the 2017 Pohang earthquake (Table 1 and Fig. 1(a)). Notably, sand boil at Site CH-2 and ground settlements and tilting of the buildings at Site CH-4 were reported from field investigations (Fig. 2; Kang et al., 2019). National Institute of Disaster and Safety (NDMI) of Korea performed five borehole tests (i.e., Sites CH-1, 2, 3, 4, and 5) to identify the liquefied ground conditions (NDMI, 2019). According to the field investigations, both Sites CH-2 and CH-4 have sand layers close to the ground surface and under the water table, which are susceptible to liquefaction during earthquakes (Fig. 1(b)). Site CH-4 shows a relatively high fines content in the top layer, and this posed a challenge to create a homogeneous layer during soil model preparation. At Site CH-1, liquefaction was observed; however, the presence of silty clay mixed with gravel and rock fragments from the surface to a depth of 4.5 m posed such challenge. Similarly, Site CH-5 shows a fine-grained sand layer that extends from the surface to a depth of 3.0 m. Such compositions were deemed impractical to achieve homogeneous ground models, and therefore, these sites were excluded. Meanwhile, Site CH-3 was also excluded because it was hardly liquefied during the 2017 Pohang earthquake. Therefore, among

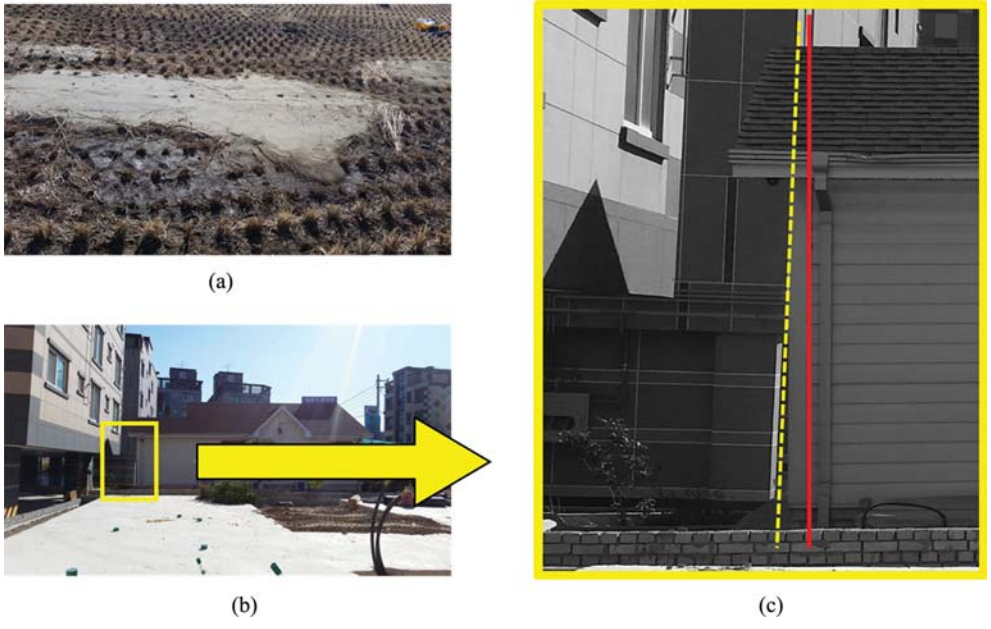

Fig. 2. Digital Photos of the Consequences of Pohang Liquefaction: (a) Sand Boil at Site CH-2, (b) Differential Settlement Near Site CH-4, (c) A Zoomed View of (b)

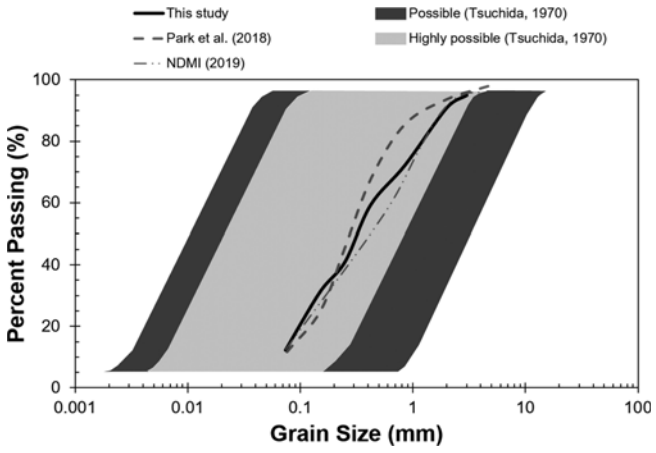

Fig. 3. Grain Size Distributions of the Soil from Site CH-2. Liquefiable Zones Based on Grain Size are Superimposed (Tsuchida, 1970; Park et al., 2018; NDMI, 2019)

Table 2. Properties of Soils Used in This Study and from the Field

Properties	Silica sand (used in this study)	Site CH-2 (field)	
		NDMI (2019)[1]	Park et al. (2018)[2]
e_{min}	0.38	-	0.68
e_{max}	0.63	-	0.97
G_s	2.65	2.75	2.5
e	0.52	-	-
D_r (%)	45	medium dense	-
d_{10} (mm)	0.065	0.045	0.065
d_{30} (mm)	0.143	0.245	0.174
d_{50} (mm)	0.318	0.459	0.276
d_{60} (mm)	0.435	0.613	0.341
d_{70} (mm)	0.746	0.875	0.456
C_u	6.7	13.6	5.2
C_c	0.7	2.2	1.4
USCS	SP	SM	SP

[1]2.5 m depth; [2]0 m depth (surface sand boil).

various sites, Site CH-2 was chosen as the model ground to be reproduced in this study.

2.2 Soil Model

In this study, we used silica sand to construct a soil model, synthesized to match the grain size distribution of the actual field soil. In particular, the particle size distribution of Site CH-2 was recreated using two field test datasets, as shown in Fig. 3 (Park et al., 2018; NDMI, 2019). Herein, the particle size distribution of Site CH-2 and the relative density at a depth of 2.5 m were obtained from the borehole tests along with soil properties in the vicinity of the sand boil. The soil sample from Site CH-2 had no fine content. As a result, the grain size distributions (GSDs) of the soil sample from the field Site CH-2 and the reproduced soil are categorized to have a high liquefaction probability according to the criterion suggested by Tsuchida (1970) (Fig. 3).

A soil model was prepared through a dry pluviation-tamping process in a rigid model container with dimensions of 11.4 × 4.6 m × 9.8 m (length × width × height). First, a sandpaper with a grain size of 0.4 mm, similar to d_{50} of the soil, was attached to the floor of the rigid model box to generate friction between the bottom of the model container and the soil (Table 2). The dry pluviation process employed a funnel to establish a uniform soil model and avoid the segregation of gravel and sand. Herein, we controlled the drop height from the funnel to achieve the desired relative density. Upon dry-pluviating to a setting lift thickness, the soil surface was hand-tamped and leveled (pluviation-tamping method) to facilitate installation of sensors. As a result, a soil model with an average depth of 5.5 m, width of 4.6 m, length of 17.1 m, and a slope angle of 5° was prepared at a prototype scale and a medium-dense condition with a relative density of 45% was achieved by the dry pluviation-tamping method. Table 2 summarizes the properties of the soil model used in this study. Note that the hand-tamping process could have resulted in layering and density gradation within a lift. However, we presumed that such effects would be minimal as the lift thickness was much less than the height of the whole soil model (0.45 m versus 5 m). This study modeled the top soil layer of CH_2 site, which is characterized as silty sand with gravel and

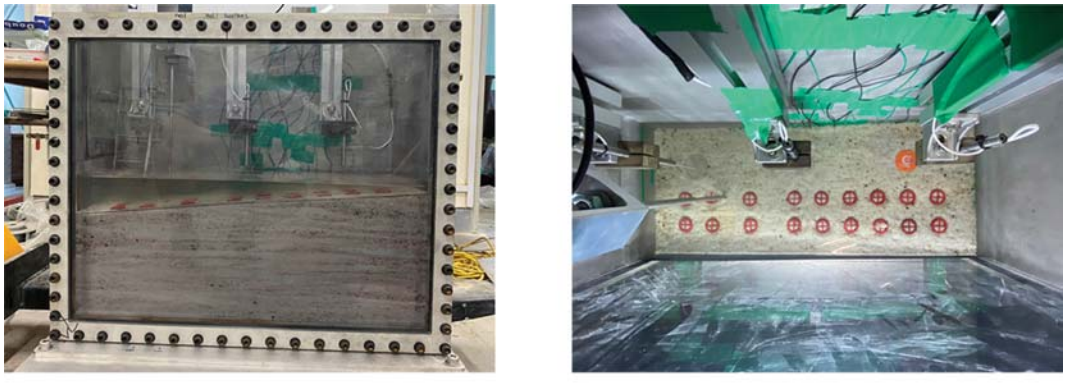

(a) (b)

Fig. 4. Digital Photos of the Soil Model: (a) Side View, (b) Plan View

stretched to a depth of 5.5 m, while the whole soil profile at Site CH-2 extends to a depth of 24 m (Fig. 1(b)). The actual CH-2 site was flat; however, the soil model was reconstituted as a sloping ground with 5° to observe lateral spreading, a representative indicator to large strain deformation induced by liquefaction, as shown in Fig. 4. The soil model physically modeled the ground to a depth of 5.5 m based on the center of the slope. The soil profile of the lower layers was used to generate seismic input motions through the one-dimensional (1D) site response analysis (SRA).

The saturation and viscosity of the pore fluids heavily affect the liquefaction phenomenon. Since a little difference in saturation can significantly impact the soil's resistance to liquefaction, the soil model was carefully saturated with a viscous fluid by using the vacuum saturation method (Yoshimi et al., 1989). We prepared a mixture of hydroxypropyl methylcellulose (HPMC) as the pore-saturating viscous fluid by using the hot/cold method (Dow Chemical Company, 2002; Adamidis and Madabhushi, 2015). To eliminate air from the soil model, circulation was carried out in a sequence as follows. The soil model was placed in the vacuum chamber, and a vacuum of -95 kPa was first achieved. CO_2 gas was then injected until the gas pressure reached +15 kPa, and the vacuum chamber was shut for 30 minutes. Thereafter, a vacuum of -95 kPa was again applied. After three cycles of this operation, the saturation process was conducted by dropping the viscous fluid at a rate of 3 – 5 mL/min under a vacuum condition. To avoid the disturbance on the soil surface by the fluid's drop energy, a nonwoven fabric sheet was put on the ground surface. The saturation procedure stopped when the fluid level reached 1 cm above the ground surface. The soil model was fully saturated with the viscous fluid, and the degree of saturation was estimated as 99.56% according to the Okamura method (Okamura and Inoue, 2012).

2.3 Input Motion

To simulate liquefaction by the 2017 Pohang earthquake in the centrifuge test, it is crucial to match not only the soil property but also the ground motion of in-situ conditions. Unfortunately, since there was no seismometer at Site CH-2, we could not obtain the ground motion of the field. Thus, we decided to simulate the ground motion at Site CH-2 through the 1D SRA for the input motion of the centrifuge test using an equivalent linear method via DEEPSOIL software (Hashash et al., 2017). The ground motion used for the base motion (= DEEPSOIL Input in Fig. 5) of 1D SRA was selected as the earthquake record measured in the North-South direction at the rock outcrop of the Pohang Old Port seismometer of the Korea Institute of Ocean Science and Technology (KIOST), which was the closest station from the epicenter (MOF, 2018; Lee et al, 2021). Based on the borehole test results for the entire soil profile of Site CH-2, a 1D SRA was conducted. Since the top layer (0 – 5.5 m depth) of Site CH-2 was designated as the soil model, we extracted the acceleration time history at 5.5 m depth as an input motion for the centrifuge experiment (= DEEPSOIL Output in Fig. 5). The results of SRA

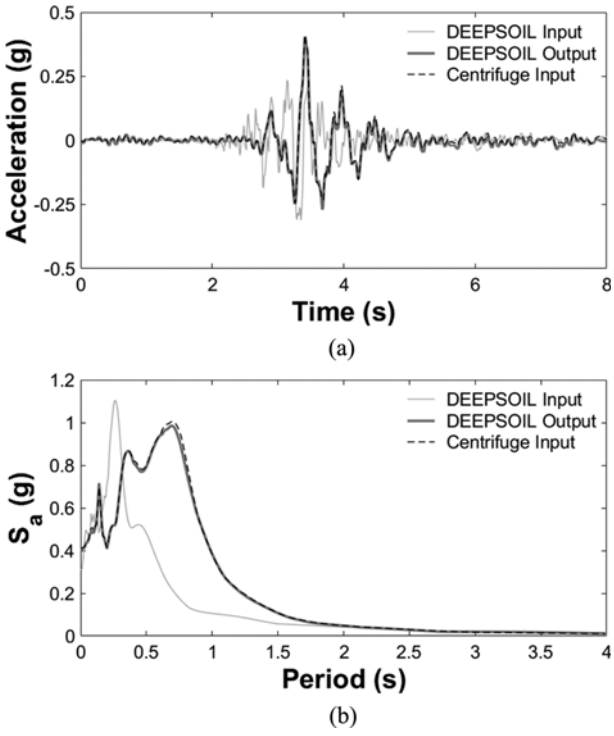

Fig. 5. The Input Motion for the Dynamic Centrifuge Experiment: (a) Acceleration Time Histories, (b) Response Spectra

(= DEEPSOIL Output in Fig. 5) and the input motion observed during the centrifuge test (= Centrifuge Input in Fig. 5) were almost identical.

In this study, we deliberately used the input motion with a lower energy than the estimated energy of the seismic response at Site CH-2. The Pohang Old Port seismometer is 7 km distant from the epicenter; however, Site CH-2 is approximately 1 km distant (Fig. 1(a)). Because the energy of ground motion attenuates with distance, the energy at the base of Site CH-2 is expected to be greater than the observed energy at the rock outcrop of the Pohang Old Port. It can be hypothesized that liquefaction would also trigger at Site CH-2 if liquefaction occurs with this input motion with the lower energy, generated based on the Pohang Old Port record.

2.4 Centrifuge Model Configuration

In the soil model, arrays of sensors were installed: 8 accelerometers (ACCs) for recording ground acceleration, 7 pore pressure transducers (PPTs) to monitor pore water pressure change, and 3 linear variable displacement transducers (LVDTs) for measuring vertical ground surface displacement. In addition, 18 markers were employed to observe the horizontal displacement on the ground surface. The CPT was carried out with a miniature cone with a diameter of 6 mm (Carey et al., 2018). The exact locations of sensors and CPT are depicted in Fig. 6.

In Fig. 6, AU is an accelerometer at the upper slope, PL is a pore water pressure transducer at the lower slope, and LM is an LVDT at the center of the slope (among the two letters, the first

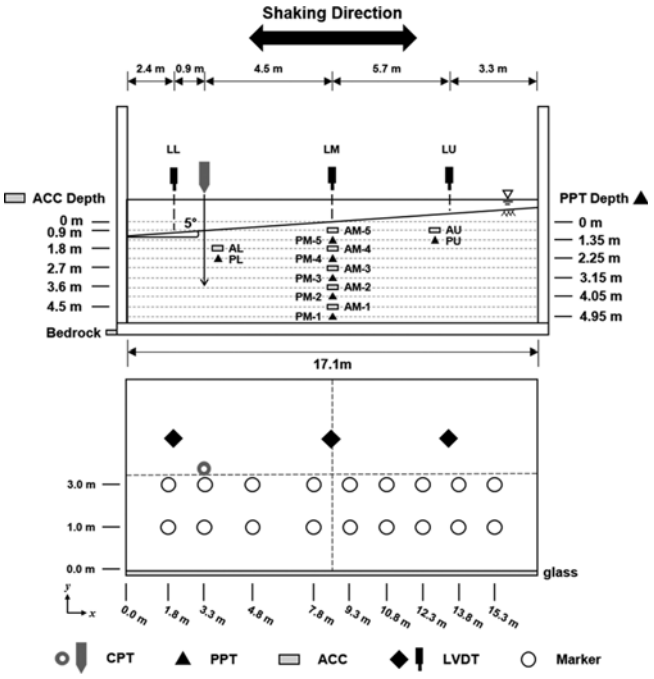

Fig. 6. Schematic Representation of the Soil Model and the Layout of Instrumentation

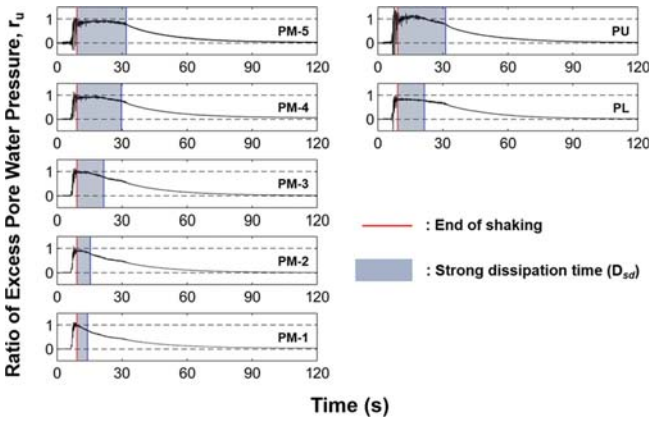

Fig. 7. Responses of the Ratio of Excess Pore Water Pressure during the Shaking

letter indicates the sensor type and the second one indicates the location). The installation depths of ACCs and PPTs were determined with reference to the slope's midpoint, and the sensor numbering followed a sequence aligned with the distance from the bottom. The installation depth of ACCs was denoted as follows: AM-5 and AU were situated at a depth of 0.9 m, and AM-4 and AL were placed at a depth of 1.8 m. As for PPTs, PM-5 and PU were installed at a depth of 1.35 m, and PM-4 and PL were positioned at a depth of 2.25 m. The markers are tracked at each position using a high-speed camera during the shaking. Subsequently, the CPT was carried out by following the test procedure in the liquefaction experiments and analysis projects (LEAP) and its recommendations (Carey et al., 2018). The cone penetrated to a depth of 3.0 m from the ground surface, considering the particle size effect, boundary effect, and penetration rate effect after the shaking (Gui and Bolton, 1998; Bolton et al., 1999).

3. Results and Analyses (I): Liquefaction Triggering

By analyzing the undrained behavior of saturated ground and the associated changes in the effective stress, liquefaction triggering during the shaking can be assessed. In this study, the response of excess pore water pressure, time history of accelerations, and changes in the shear stress-strain relationship and the spectral density were used to determine liquefaction triggering and occurrence.

3.1 Excess Pore Water Pressure

The excess pore water pressure ratio, r_u is the most representative engineering parameter to evaluate the liquefaction, and it is defined, as follows:

$$r_u = \frac{\Delta u_{ex}}{\sigma_{vo}'}, \tag{1}$$

where σ_{v0}' is the initial vertical effective stress and Δu_{ex} is the excess pore water pressure. Generally, the r_u value close to 1.0 can be considered that liquefaction has occurred, which we also regarded in this study. According to this, it is clear that liquefaction has been triggered at all locations in Fig. 7. However, it is necessary to precisely assess the degree to which soil has been liquefied to estimate the damage level and prevent potential destruction. Therefore, in cases where r_u reaches 1.0 only for a very short moment, such as PM-1 and PM-2, it is necessary to observe more closely.

When liquefaction is triggered, the excess pore water pressure persists for a long time, even after the shaking has ended, which indicates that significant shear strength instability or liquefaction damage is possible. At this time, the r_u tends to continue above 0.8 for a certain time due to upward flow from below the PPTs. Based on this feature, the interval from the end of the shaking to the point when r_u is greater than 0.8 was determined as the strong dissipation time (D_{sd}). The D_{sd} was 4.9, 6.2, 12.4, 20.5, and 22.7 s (at PM-1 to PM-5 in that order). Additionally, the D_{sd} was 12.3 and 22.1 s at PL and PU, respectively. The D_{sd} is maintained longer as the depth is shallower, implying that the pore fluid is dissipated to the surface. Particularly in the case of PL, it can be seen that the D_{sd} length is shorter than that of PU and PM-5 because less pore fluid is trapped below the soil than in the cases of PU and PM-5. PL demonstrates reduced trapped fluid below the soil compared to PM5 and PU, with the following assumptions: 1) a uniform void structure within the soil, 2) vertical fluid flows towards the surface during liquefaction. Considering this premise, when liquefaction is triggered, the thicker the liquefiable ground, the greater the amount of pore fluid that can flow to the ground surface. In other words, it can be inferred that the thicker the liquefiable ground, the more likely r_u 1.0 will be sustained for a longer duration.

As depicted in Fig. 6, PL is situated at a greater depth relative

to PM-5 and PU. Consequently, when liquefaction is triggered, the thickness of the ground, which can contain pore water fluid passing through the PPT, will be 3.25 m for PL, while for PM-5 and PU, it reaches 4.15 m. Therefore, assuming that all voids are homogeneously filled with fluid, PL inevitably has a smaller amount of upward fluid than PM-5 and PU, so there is a difference in D_{sd}.

The parameter called the ratio of dissipation time (R_{dsp}) was proposed to consider both D_{eq}, the duration of the ground motion, which is the time to apply energy to the ground, and the D_{sd}. In other words, the response of the soil system can be quantified based on the pore water pressure.

$$R_{dsp} = \frac{D_{sd}}{D_{eq}} \tag{2}$$

We evaluated whether liquefaction has triggered depending on whether R_{dsp} is 4.0 or higher. As a result, the R_{dsp} of PM-3, PM-4, PM-5, PU, and PL were determined to be 4.27, 7.09, 7.86, 4.26, and 7.64, respectively. This means that the probability that liquefaction has been triggered at the corresponding location is very high. In this study, the R_{dsp} standard was set at 4.0. However, this may vary depending on site conditions and earthquake duration. Therefore, when you use the R_{dsp} as a standard of triggering of liquefaction, we recommend thinking carefully and considering other engineering parameters together. Additionally, there is uncertainty that the r_u is inaccurate owing to a variety of experimental errors. For example, even when liquefaction has actually triggered, it is occasionally seen that r_u does not approach or exceed 1.0. This is because the PPT was not installed at the correct depth, or its position changed when an input motion was applied to generate liquefaction, resulting in an inaccuracy in the initial vertical effective stress value (Figel and Kutter, 1994; Hayden et al., 2015). Furthermore, the vertical equilibrium of the soil body may be disturbed by the acceleration transmitted in the vertical direction, enabling r_u to exceed 1.0 (Hughes and Madabhushi, 2018). As a result, it can be shown that determining the triggering of liquefaction should be conducted using a variety of approaches as well as excess pore water pressure.

3.2 Acceleration

The ground behaves like liquid when liquefaction takes place, and the seismic response is likewise significantly influenced. This phenomenon is because the ground in a loose state goes beyond the phase transformation line while experiencing cyclic loading, and the effective stress becomes zero as it crosses the contractive zone and dilative zone, as shown in Fig. 8. Because of this transition, two characteristics appear in the seismic response: 1) a flat response indicating a condition in which the acceleration response is zero during the shaking, and 2) a dilation spike indicating an abrupt acceleration response with the flat response state, which is a condition that rises suddenly and momentarily, as shown in Fig. 9. These characteristics are not present in AM-1 and AM-2 where liquefaction was not observed in the previous section. On the other hand, it can be observed that both characteristics

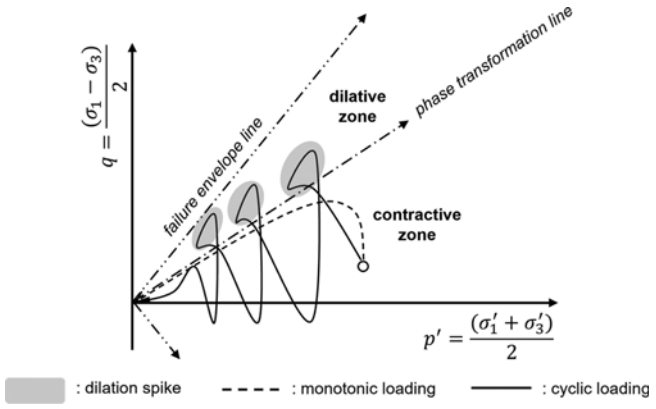

Fig. 8. A Conceptual Diagram of Undrained Soil Behavior

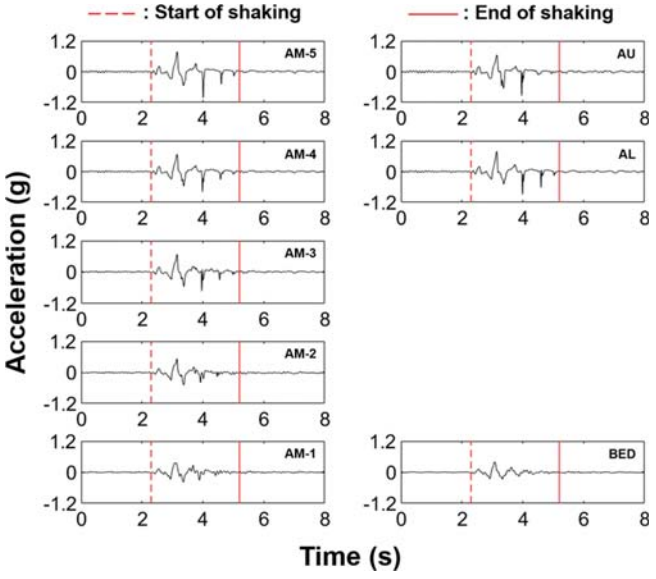

Fig. 9. Acceleration Time Histories at Various Depths during the Shaking

are present clearly in AM-3, AM-4, AM-5, AL, and AU, just like in the evaluation result of the previous section. These two characteristics can be explained as follows. First, when the earthquake occurs, the excess pore water pressure increases under such rapid cyclic loading, causing a decrease in the effective stress and a loss of shear strength of the ground. As a result, the shear modulus approaches zero, and the shear wave is not transmitted at the corresponding depth (i.e., a flat response appears). By contrast, the shear modulus increases dramatically as the effective stress increases when the soil passes its phase transform line and tends to dilate. As shear waves overlap, a response such as an impact load occurs, and this comment demonstrates a dilation spike (Ishihara et al., 1975; Alarcon Guzman et al., 1988).

3.3 Shear Stress-Strain

In the previous sections, the triggering of liquefaction was observed based on responses of the excess pore water pressure and acceleration. In this section, the occurrence of liquefaction was assessed by examining the shear stress and shear strain

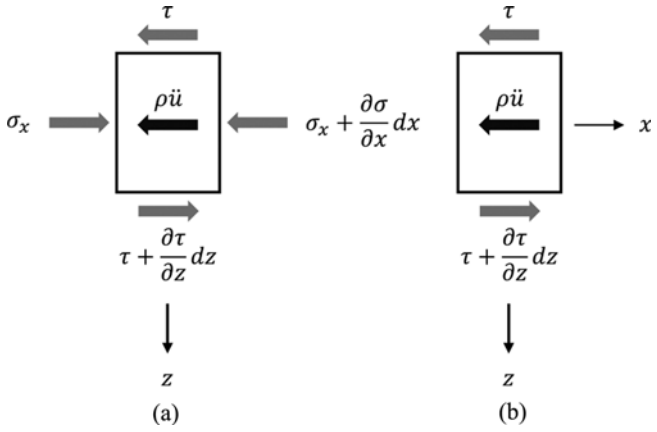

Fig. 10. Stress Configurations in a Sloping Ground Tested within a Rigid Container: (a) General Configuration, (b) Approximated Configuration along the Central Axis (Zeghal et al., 2018)

during the shaking. For this purpose, the method proposed in the LEAP was used as follows (Zeghal et al., 2018). Using the vertical arrays, accelerations have been recorded to derive nonparametric estimates of shear stress and strain histories for both level ground and infinite slope models (Zeghal et al., 1995; Elgamel et al., 1996). The evaluation of shear stresses and strains involved examining different depths on horizontal planes for level ground and along the slope for infinite slopes. This methodology employs a shear beam conceptualization to describe lateral responses in a level deposit or infinite slope. Although the shear beam assumption is not strictly applicable to this study, which utilized a rigid container, the soil response can reasonably conform to a plane strain condition, representing both lateral and vertical directions or the plane in Fig. 6.

$$\frac{\partial \sigma}{\partial x}+\frac{\partial \tau}{\partial z}=\rho \ddot{u} \tag{3}$$

Consequently, the equation of motion in the lateral direction is formulated as shown in Fig. 10 (Eq. (3)), where x and z represent coordinates in the lateral and vertical directions, u denotes total displacement in the x direction with respect to time, $u = u(x, z, t)$, $\ddot{u}$ signifies the corresponding total acceleration, $\partial^2 u/\partial t^2$, and $\sigma = \sigma_{xx}(x, z, t)$ and $\tau = \sigma_{xz}(x, z, t)$ represent normal and shear stresses acting on a soil element in the x direction, respectively.

$$\frac{\partial \tau}{\partial z}=\rho \ddot{u}\text{ , with boundary condition }\tau(0,t)=0 \tag{4}$$

Stress variations along the x direction are expected to decrease with distance from the rigid boundaries, reaching a minimum around the mid-length vertical axis. Along this axis (corresponding to vertical array AM-1 to AM-5), presumed to be considerably smaller than the variation of shear stresses along the vertical axis ($\partial\sigma/\partial x \ll \partial\tau/\partial z$), the lateral response is approximated using a one-dimensional shear beam model (Eq. (4)).

$$\tau(z,t)=\int_0^z \rho \ddot{u}(\zeta,t)\, d\zeta \tag{5}$$

Integrating this equation and applying the stress-free surface boundary condition (Eq. (4)), the shear stress at any level z can be determined (Eq. (5)).

$$\tau_i(t)=\tau_{i-1}(t)+\rho\frac{\ddot{u}_{i-1}+\ddot{u}_i}{2}\Delta z_{i-1}\text{ , }i=2,3,\ldots \tag{6}$$

Linear interpolation between accelerations of a vertical array (e.g., AM-1 to AM-5 in Fig. 6) reduces the discrete equivalent of shear stress at level z_i of the i^{th} accelerometer (Eq. (6)).

$$\tau_{i-1/2}(t)=\tau_{i-1}(t)+\rho\frac{3\ddot{u}_{i-1}+\ddot{u}_i}{2}\Delta z_{i-1}\text{ , }i=2,3,\ldots \tag{7}$$

At the midpoint between levels z_{i-1} and z_i, shear stress can be expressed accordingly (Eq. (7)).

$$\gamma=\frac{\partial u}{\partial z} \tag{8}$$

Corresponding shear strains γ are given by (Eq. (8)), and shear strain γ_i at levels z_i and $(z_{i-1} + z_i)/2$ can be expressed as shown (Zeghal et al., 1995) (Eqs. (9) and (10)).

$$\gamma_i(t)=\frac{1}{\Delta z_{i-1}+\Delta z_i}\left(\frac{u_{i+1}-u_i}{\Delta z_i}\Delta z_{i-1}+\frac{u_i-u_{i-1}}{\Delta z_{i-1}}\Delta z_i\right)\text{ , }i=2,3,\ldots \tag{9}$$

$$\gamma_{i-1/2}(t)=\frac{u_i-u_{i-1}}{\Delta z_{i-1}}\text{, }i=2,3,\ldots \tag{10}$$

To calculate stresses (Eqs. (6) and (7)), first-order linear interpolation was applied between accelerations, while second-order interpolation between displacements was used to assess strains (Eqs. (9) and (10)). These interpolations offer consistent stress and strain approximations of second-order accuracy (Zeghal and Elgamal, 1993; Zeghal et al., 2018).

The normalized acceleration response and the r_u response were plotted overlaid by depth, then divided into four-time steps: T1 (0 – 2.3 s) in the state before the input motion is applied, T2 (2.3 – 3.5 s) is the state of shaking, but the r_u did not reach to 1.0; T3 (3.5 – 5.2 s) is the state after the r_u reached to 1.0 during the shaking; Finally, in T4 (> 5.2 s), the input motion was terminated but still liquefied condition, which is the post liquefaction (Fig. 11(a)). The black line represents the acceleration response, and the gray line represents the r_u response. In T2, the input motion is applied, causing the acceleration response to emerge and an increase in the excess pore water pressure. When the r_u reached 1.0 at 3.5 s, liquefaction is triggered, as indicated in T3, and the consequence can be seen in the acceleration response. The effective vertical stress converges to zero, and the flat response, in which the acceleration response does not manifest, can be identified in A/PM-3, A/PM-4, and A/PM-5. Also, a dilation spike appears in the acceleration response when the r_u is momentarily decreased. Finally, in T4, the acceleration response disappears due to the end of the shaking, and only the excess pore water pressure persists.

The nonparametric estimation of shear stress and strain histories has been derived from the accelerometers at AM vertical arrays.

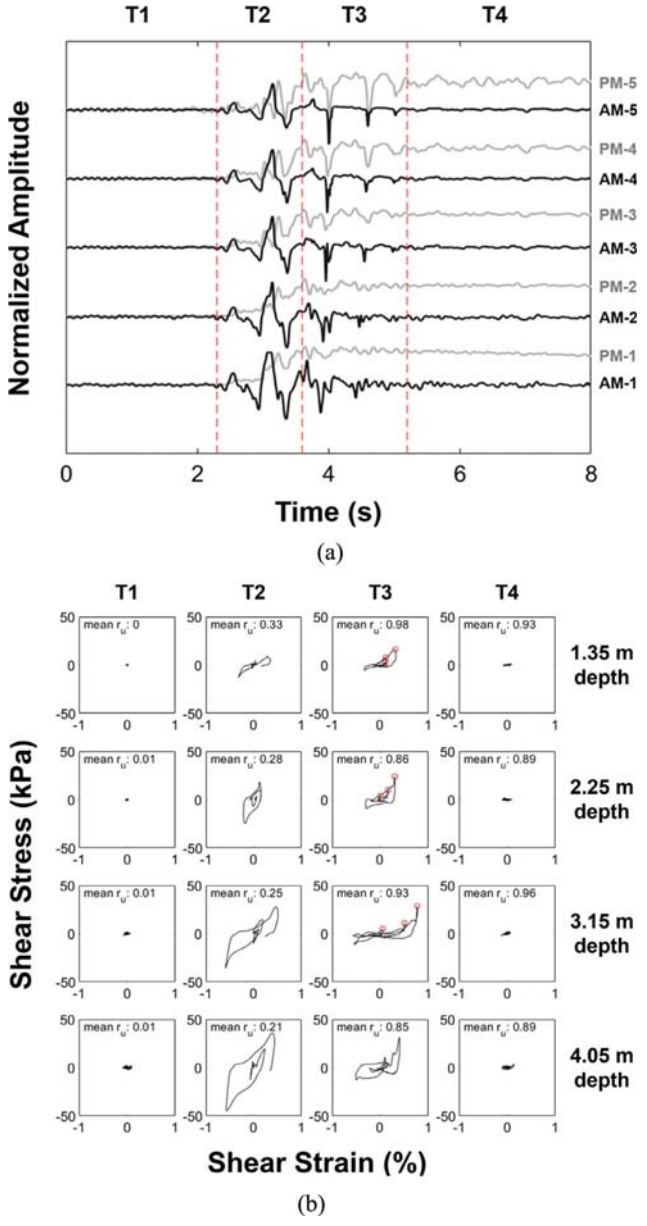

Fig. 11. Triggering of Liquefaction with Time: (a) Comparison of Normalized Acceleration and Excess Pore Water Pressure, (b) Shear Stress-Strain Curves at Various Times and Depths

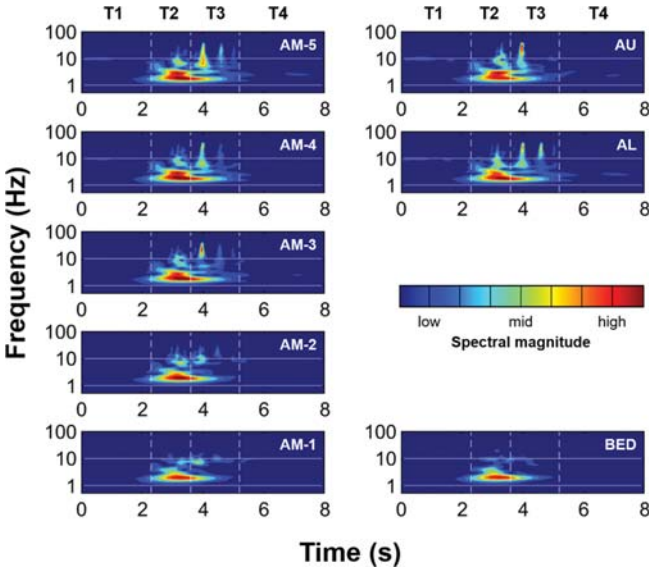

Fig. 12. Time-Frequency Analysis Results by Using Stockwell Transformation

In T2, the wave energy started to be transmitted to the ground as the input motion started to excite. But, since the average r_u did not reach 1.0, it can be seen that the shear stress was transmitted to the ground at all depths. On the other hand, in T3, as the average r_u approaches almost 1.0, liquefaction is triggered, representing a zero effective stress state. In addition, compared to the shear modulus at T2, which is the slope of the backbone curve, the shear modulus is almost zero at T3. Therefore, a flat response is shown in this state, and a dilation spike, denoted by a red circle, develops when the shear strength is temporarily restored. Nevertheless, it is evident that liquefaction did not manifest entirely at a depth of 4.05 m in T3. This observation is attributed to the fact that the backbone curve not only exhibited an incomplete zero effective stress state in comparison to the curve at a depth of 3.15 m but also demonstrated a lower average r_u value. Lastly, in T4, liquefied condition, but no motion is transmitted to the ground so that no characteristics can be seen.

3.4 Time-Frequency Analysis

As previously mentioned, liquefaction causes the ground to soften, and as a result, the ground's frequency response to an earthquake transforms as follows: a low-frequency band predominantly develops in a section where the effective stress of the soil is diminished; a high-frequency peak emerges at the moment when the effective stress is recovered. Using these characteristics, previous studies used time-frequency analysis to identify the exact time of liquefaction initiation (Kramer et al., 2016; Karimi et al., 2018; Macedo and Bray, 2018). To observe this point, the acceleration response in the ground was analyzed in the time-frequency domain using the S-Transform (Fig. 12). The Stockwell transformation, or S-Transform, is a time-frequency analysis method for simultaneously representing signals in both the time and frequency domains. It differs from the Short-Time Fourier Transform (STFT) and Continuous Wavelet Transformation (CWT) by using adaptive windows that vary with frequency, making it well-suited for analyzing signals with changing spectral characteristics. The result is a spectrogram that shows the signal's time-varying frequency components, making it useful to observe the triggering of liquefaction (Stockwell et al., 1996; Özener et al., 2020). As a result, a high-frequency peak (dilation spike), which was above 10 Hz, that emerged at around 4.0 s at the locations of AM-3, AM-4, AM-5, AL, and AU was identified compared to the bedrock response. However, the development of the low-frequency band as a result of the flat response was not noticeable. This is because the earthquake duration used as the input motion was short, and therefore the time for the seismic motion to be transmitted to

the ground after liquefaction was short. Consequently, based only on time-frequency analysis, the timing of liquefaction could be estimated as about 4.0 s. Although there was a slight delay between the result of r_u and the liquefaction initiation time, which was 3.5 s, it was still feasible to predict nearly the same time. Therefore, the timing of the liquefaction could be roughly identified by the seismograph even when the piezometer is not installed in the actual field.

4. Results and Analyses (II): Deformations from Liquefaction

Applying diverse investigative methods, it was observed that liquefaction had been triggered; however, the key manifestation, the sand boil, was not apparent at the surface. The sand boil phenomenon is typically noticeable in regions with a significant concentration of excess pore water pressure near the surface, especially in soil profiles that consist of alternating permeable and impermeable layers. Alternatively, it can occur in situations where the upper layer is impermeable. However, the soil employed in this study is a homogenous sand layer, which is chanllenge to observing a sand boil. This is because excess pore water pressure is uniformly dissipated across the entire layer, making it difficult to pinpoint a concentrated point of observation (Wang, 2021).

Hence, in this section, we predominantly delved into the consequences of liquefaction, particularly highlighting settlement and lateral spreading.

4.1 Vertical Displacement

In general, ground settlement happens when liquefaction is triggered. This is because the particle arrangement in the ground is replaced with the denser ground when pore water escapes and rearranges owing to the earthquake. The experimental results also showed a similar pattern. It can be seen that, in the middle and upper parts of the slope, LM and LU, immediately after the input motion is loaded, the excess pore water pressure is developed, and settlement occurs (negative direction) (Fig. 13(a)). On the other hand, the lower part of the slope in LL rose (positive direction) and then settled (negative direction) owing to liquefaction after the input motion has loaded. This is because it was located at the bottom of the slope, the soil at the top and middle of the slope was swept down to the bottom by lateral spreading that occurred during liquefaction.

4.2 Horizontal Displacement

The horizontal displacement was measured by scanning the markers on the ground surface with a high-speed camera during the shaking. The amount of displacement measured in this way is

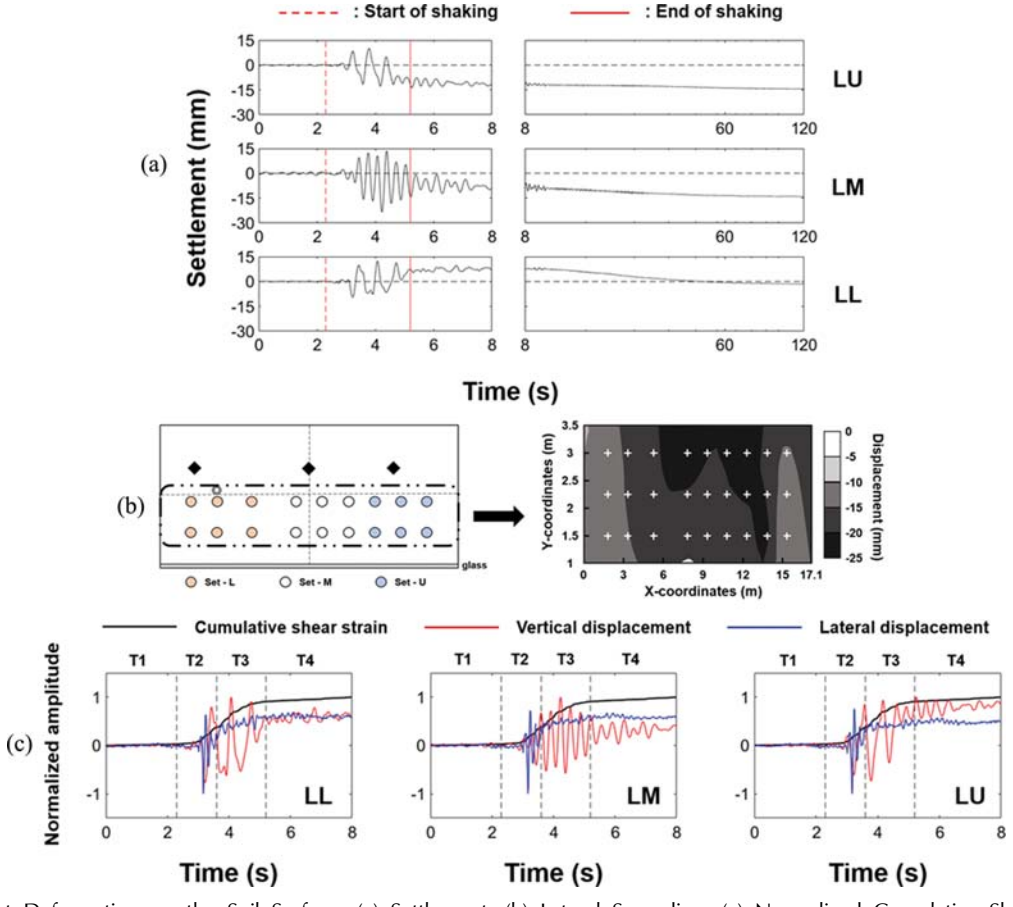

Fig. 13. Permanent Deformation on the Soil Surface: (a) Settlement, (b) Lateral Spreading, (c) Normalized Cumulative Shear Strain-Vertical Displacement-Horizontal Displacement

shown as a contour line in Fig. 13(b). Here, a negative value means that horizontal displacement has occurred to the left side (lower part) of the slope. The upper part of the slope occurred the most, followed by the middle part, and the lower part occurred the least, according to the analysis. This pattern matches the above-mentioned vertical displacement results.

4.3 Cumulative Shear Strain

The cumulative shear strain was calculated from the shear strain results acquired in the shear stress-strain part of the liquefaction evaluation. Since the shear strain results vary based on depth, all the shear strains for each depth were summed and normalized to the maximum value. Additionally, the cumulative shear strain was plotted in the time domain alongside the vertical and horizontal displacements normalized to their maximum value (Fig. 13). At this point, the horizontal displacement case, as shown in Fig. 13(b), was compared with LL and Set-L, LU and Set-M, and LU and Set-U. Additionally, for trend comparison, the cases of LM and LU were reversed after normalization (i.e., the settlement is in the negative direction in LL but in the positive direction in LM and LU).

$$Cumulative\ Shear\ Strain = \frac{\int|\gamma(t)|dt}{\max(\int|\gamma(t)|dt)}, \quad (11)$$

where $\gamma(t)$ is shear strain and t is time.

Comparing the normalized amplitude by the sensor location and time indicated that cumulative shear strain started to increase at T2 and T3, approximately reached a steady state at T4, and both vertical and horizontal displacements showed similar deformation results. This indicated that lateral spreading, one of the most apparent ground surface evidence of liquefaction, occurred concurrently with the settlement. This phenomenon occurs when the shear strength for the liquefied state is greater than the shear stress for static equilibrium, and deformation is developed incrementally.

5. Discussion

5.1 Comparison with Previous Approaches

When assessing the potential for liquefaction, a critical factor is accurately identifying critical depths, most susceptible to liquefaction. This determination is paramount, as it allows for applying the most efficient and cost-effective ground improvement methods to mitigate the risk of liquefaction.

This section analyzes the experiment's results using various liquefaction evaluation criteria suggested in previous studies (Takada and Ozaki, 1997; Suzuki et al., 1998; Yamamoto et al.,

Table 3. Comparison of Previous Methods for Liquefaction Prediction

Analysis methods	Evaluation parameters		Criteria	BED	AM-1 PM-1	AM-2 PM-2	AM-3 PM-3	AM-4 PM-4	AM-5 PM-5	AL PL	AU PU
This study	Ratio of excess pore water pressure		≈ 1.0	-	O	O	O	O	O	O	O
	Ratio of dissipation time		≥ 4.0	-	X	X	O	O	O	O	O
	Flat response and Dilation spike		Presence	X	X	X	O	O	O	O	O
Takada and Ozaki (1997)	PGA (cm/s^2)	$max(a(t))$	≥ 100	397 O	355 O	518 O	664 O	659 O	764 O	770 O	639 O
	SI_{max} (cm/s)	$max\left(\frac{1}{2.4}\int_{0.1}^{2.5} S_V(T,\xi)dT\right)$	≥ 20	2895 O	3559 O	3960 O	4571 O	4765 O	5430 O	4796 O	4870 O
	D_c (cm)	$\frac{2SI^2}{PGA}$	≥ 10	42187 O	71266 O	60477 O	62886 O	68844 O	77115 O	59753 O	74239 O
Suzuki et al. (1998)	R_L	$FS(\omega) = \left[\left\{\int_0^T a(t)\sin\omega t\ dt\right\}^2 + \left\{\int_0^T a(t)\cos\omega t\ dt\right\}^2\right]^{\frac{1}{2}}$	≥ 0.25	0.28 O	0.26 O	0.28 O	0.28 O	0.26 O	0.25 O	0.26 O	0.25 O
	$F_{p,a}$ (Hz)		≤ 1	1.86 X	1.86 X	1.86 X	1.86 X	1.66 X	1.66 X	1.66 X	1.86 X
Yamamoto et al. (1999)	$R_{I\,0.85}$ $R_{I\,0.95}$	$I_a = \frac{\pi}{2g}\int_0^{T_0} a(t)^2$	≥ 0.6: **F**ull ≥ 0.3: **P**artial	0.90 F 0.65 F	0.86 F 0.62 F	0.84 F 0.61 F	0.84 F 0.58 P	0.85 F 0.57 P	0.82 F 0.55 P	0.82 F 0.56 P	0.80 F 0.51 P
Kostadinov and Yamazaki (2001)	PGV (cm/s)	$max(v(t))$	≥ 10	21.18 O	26.04 O	28.98 O	33.44 O	34.86 O	39.73 O	35.09 O	35.63 O
	MIF (Hz)	$\frac{\int fP(t,f)df}{\int P(t,f)df}$	≤ 1.0 : **F**ull ≤ 1.5 : **P**artial	- X	- X	- X	- X	- X	- X	- X	- X

1999; Kostadinov and Yamazaki, 2001). Each analysis method was named after the researcher: 1) Takada and Ozaki's method: peak horizontal ground acceleration (*PGA*), maximum spectrum intensity (SI_{max}), Maximum horizontal ground displacement (D_c); 2) Suzuki's method: ratio of low-frequency portion to the whole area of the Fourier amplitude spectrum (R_L), averaged predominant frequency ($F_{p,a}$); 3) Yamamoto's method: ratio of Arias intensity of filtered to non-filtered acceleration time history (R_I); and 4) Kostadinov and Yamazaki's method: peak horizontal ground velocity (*PGV*), mean instantaneous frequency (*MIF*).

The formula of main evaluation parameters and their values at each location are briefly described in Table 3. In Table 3, 'O' means that liquefaction is triggered by meeting the relevant evaluation criteria, and 'X' means that liquefaction is not triggered. In the case of the Takada and Ozaki method, the ground can be evaluated as liquefied condition, regardless of sensor location. In the case of Suzuki's method, the ratio of the low-frequency portion to the whole area of the Fourier amplitude spectrum satisfies the criteria regardless of location. But, the averaged predominant frequency exceeds the criteria at the entire location. Yamamoto's method shows that the ground was fully liquefied when the steepness, related to the length of the transition zone when applying the lowpass filter, was 0.85. However, in the case of the steepness value being 0.95, the ground was evaluated as a partially liquefied condition at a close surface. Similar to Suzuki's method, the mean instantaneous frequency does not meet the requirements. In contrast, the peak horizontal ground velocity measurements satisfy Kostadinov and Yamazaki's method (Fig. 14). As observed, it fails the frequency-related requirement compared to the previous approaches. This is related to the reason that the input motion's duration was considerably shorter in this study than it was in the approach that preceded previously.

By applying the liquefaction triggering criteria presented in previous studies to this research, it is concluded that liquefaction is triggered regardless of depth. This is due to the proposed techniques dominantly capturing ground motion characteristics. However, based on the criteria stated in this study, it is estimated that the soil was liquefied until the depths of AM-3 and PM-3 from the surface. In other words, if only the ground motion characteristics are considered to determine the triggering of liquefaction, the results can be overestimated. This shows that completely different results can be obtained, like the duration of the earthquake is very short, as in the case of the 2017 Pohang liquefaction. Therefore, it is clear that to identify the depth to which it liquefied precisely, consideration should be given to the excess pore water pressure and the characteristics of the earthquake.

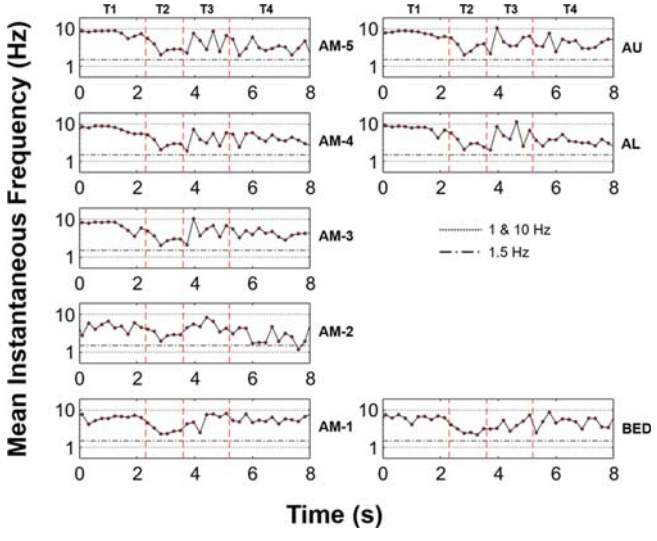

Fig. 14. Responses of the Mean Instantaneous Frequency Obtained from the Time-Frequency Analysis

5.2 Comparison of Factor of Safety: Field versus Centrifuge

The primary purpose of this research is focused on reproducing the 2017 Pohang liquefaction at the CH-2 site. The in-situ SPT and the centrifuge CPT results are juxtaposed through the application of the liquefaction factor of safety, FS_{liq}. This facilitates a comparative analysis of the centrifuge results' trends with those obtained from the field test. Therefore, the FS_{liq} values acquired during the field SPT test were given in the NDMI report (2019), and centrifuge CPT was conducted before and after the input motions at the locations depicted in Fig. 6.

For calculating the FS_{liq}, the simplified method is considered, which method was originally developed by Seed and Idriss (1971) and continuously modified by several researchers (Robertson and Wride, 1998; Youd et al., 2001; Cetin et al., 2004; Boulanger and Idriss, 2014; Cetin et al., 2018). The FS_{liq} is the ratio of cyclic resistance ratio (*CRR*) to cyclic stress ratio (*CSR*), and if FS_{liq} is larger than 1.0, then it is evaluated that liquefaction can be triggered:

$$FS_{liq} = \frac{CRR_{M_w=7.5,\ \sigma_v'=1}}{CSR_{M_w=7.5,\sigma_v'=1}/(MSF \times K_\sigma)}, \tag{12}$$

where the *CRR* is resistance to liquefaction at the moment magnitude is 7.5 and 1 atm, and the *CSR* is shear stress induced by the earthquake at the moment magnitude is 7.5 and 1 atm. The *MSF* is the magnitude scaling factor, and the K_σ is the overburden correction factor.

The *CSR* follows as (Seed and Idriss, 1971):

$$CSR = 0.65\frac{\tau_{max}}{\sigma_v'} = 0.65\frac{a_{max}}{g}\frac{\sigma_v}{\sigma_v'}r_d, \tag{13}$$

where the τ_{max} is maximum shear stress at depth induced by the earthquake, the σ_v' is effective vertical stress at depth, the a_{max} is the maximum acceleration at the surface (here, we use the response from AM-5 which is 0.41 g), the g is gravitational acceleration, the σ_v is total vertical stress at depth, and the r_d is a shear stress reduction factor which suggested by Idriss and Boulanger (2006).

The *CRR* is suggested by Robertson and Wride (1998) (Eq. (14)) and Boulanger and Idriss (2014) (Eq. (16)), as follows:

$$CRR_{7.5} = 0.833[q_{c1Ncs}] + 0.05 \quad \text{if, } q_{c1Ncs} < 50, \tag{14}$$

$$CRR_{7.5} = 93[q_{c1Ncs}/1000]^3 + 0.08 \quad \text{if, } 50 \le q_{c1Ncs} \le 150\,, \tag{15}$$

$$CRR_{M_W=75,\,\sigma_v'=1} = \exp\left\{\frac{q_{c1Ncs}}{113} + \left(\frac{q_{c1Ncs}}{1000}\right)^2 - \left(\frac{q_{c1Ncs}}{140}\right)^3 + \left(\frac{q_{c1Ncs}}{137}\right)^2 - 2.8\right\}, \tag{16}$$

$$q_{c1Ncs} = C_N \times q_c / P_a\,, \tag{17}$$

$$C_N = (P_a/\sigma_v')^{0.5}\,, \tag{18}$$

where q_{c1Ncs} is the corrected cone penetration resistance value for overburden stress and clean sand, q_c is cone penetration resistance, C_N is overburden correction factor, and P_a is atmosphere pressure (Liao and Whitman, 1986; Youd et al., 2001; Boulanger, 2003; Cetin et al., 2004, 2018; Moss, 2006; Idriss and Boulanger, 2006; Boulanger and Idriss, 2014; Boulanger and Idriss, 2015).

In the centrifuge experiment, CPTs were performed once before and once after shaking. The observed increase in q_c post-liquefaction, in comparison to the pre-liquefaction values, suggests that soil densification occurred due to particle redistribution following liquefaction. As a consequence, by using the *CRR* calculation approach, FS_{liq} was evaluated in two different methods (Fig. 15). According to Boulanger and Idriss's methodology (2014), the result is shown in Fig. 15(b), and Robertson and Wride's methodology (1998) provided a result as shown in Fig. 15(c). The FS_{liq} before the liquefaction is shown by the solid line, while the FS_{liq} after the liquefaction is represented by the dotted line (Fig. 15(d)). The observed increase in the FS_{liq} value after liquefaction is likely a consequence of particle rearrangement, where the dissipation of fluid previously trapped in the pores during the liquefaction process contributes to this phenomenon. Notably, the FS_{liq} value derived from the in situ SPT data, depicted by the black dotted line, closely parallels the centrifuge CPT result. This alignment implies the successful execution of physical modeling in this study. However, since there are discrepancies between field and centrifuge test conditions (e.g., void ratio, boundary condition, etc.), it is cautious approach to evaluate liquefaction using only the test results presented in this study.

6. Limitation

In this section, despite our endeavors to enhance the precision of physical modeling for the 2017 Pohang liquefaction, we have explicitly outlined the existing limitations:

1. Disparities in soil properties between Site CH-2 and the soil used in the centrifuge experiment: Ideally, it would have been beneficial to employ undisturbed soil samples directly from Site CH-2, where liquefaction was observed in the field, for the centrifuge experiment. Nonetheless, since Site CH-2 is a private area, acquiring enough soil for the experiment was difficult. Consequently, we synthesized silica sand with a GSD similar to that of the field soil based on data from NDMI (2019) and Park et al. (2018).
2. Boundary effect of the rigid container: The model container used in the centrifuge experiment, being a rigid container, may induce reflections of seismic waves and affect pore water pressure dissipation due to differences in dynamic characteristics between the container and the soil model with input motion. These boundary effects could influence the assessment of liquefaction occurrence. In this study, to take these into account, we applied not only the ratio of excess pore water pressure but also considered acceleration time histories, shear stress-strain responses, and time-frequency histories in the evaluation of liquefaction. This comprehensive approach was implemented to minimize potential misinterpretations arising from the effects of

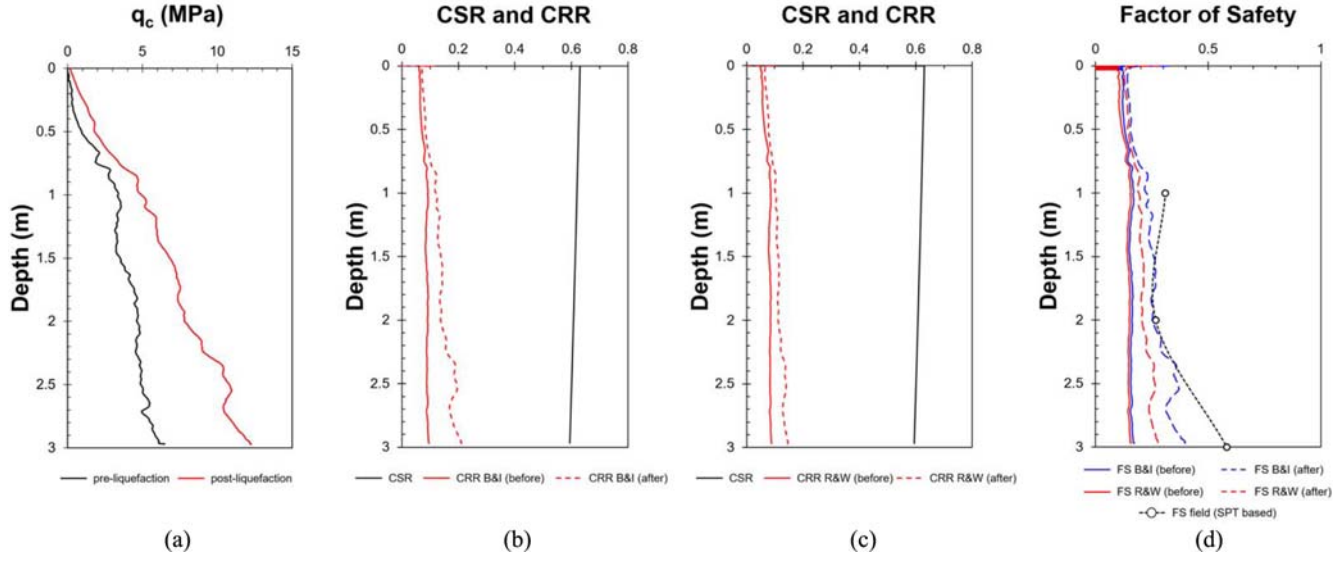

Fig. 15. The Factor of Safety for Liquefaction (FS_{liq}): (a) Cone Penetration Resistances, (b) *CSR* and *CRR* Curves by Boulanger and Idriss (2014), (c) *CSR* and *CRR* Curves by Robertson and Wride (1998), (d) Comparison of FS_{liq} between Centrifuge and Field

boundary condition.

7. Conclusions

This research successfully replicated liquefaction induced by the 2017 Pohang earthquake, contributing to the development of frameworks for predicting and mitigating future liquefaction-induced damage. Several significant findings emerged as well:

1. Centrifuge Modeling and Site Response Analysis: The study utilized centrifuge modeling based on the 2017 Pohang liquefaction, employing input motions generated from site response analysis. The soil model faithfully replicated field conditions, facilitating a comprehensive investigation.
2. Assessment of Liquefaction Triggering: Evaluation of liquefaction occurrence was achieved by measuring the ratio of excess pore water pressure. However, acknowledging the potential for overestimation, a criterion based on the dissipation time of excess pore water pressure and the ratio of excess pore water pressure was proposed to assess liquefaction more accurately.
3. Validation of Liquefaction Triggering:
   1) Analysis of acceleration time history identified distinct features indicating liquefaction: a flat response due to shear strength converging to zero and a dilation spike from rapid, effective stress recovery.
   2) Shear Stress-Strain Relationship: The shear stress-strain relationship validated the liquefaction mechanism, demonstrating almost zero shear stress as the effective stress state approached zero at the fully liquefied moment.
   3) Dynamic Time-frequency Response: The analysis observed differences in dynamic response of soil between cases where liquefaction is triggered and where it did not, particularly in the high-frequency band.
4. Consequences of Liquefaction: The consequences, including horizontal and vertical displacement, were evident. Different behaviors were observed in different conditions, with settlements, uplift, and surface deformation correlating with shear strain development.
5. Comparison with Previous Research: Comparison of liquefaction criteria with previous methodologies highlighted potential overestimations in other approaches compared to those utilized in this study, emphasizing the importance of considering excess pore water pressure.
6. Evaluation of Factor of Safety for liquefaction (FS_{liq}): FS_{liq} was evaluated using simplified method for data from SPT and centrifuge CPT at the location of actual liquefaction. While slight underestimation was noted in the centrifuge, the overall pattern matched well with actual conditions.

In conclusion, this research contributes significantly to understanding liquefaction phenomena. It establishes basic methodologies for accurate prediction, assessment, and mitigation of liquefaction-induced ground damage, emphasizing the necessity of considering excess pore water pressure and dynamic ground response characteristics. The study's findings provide valuable insights for future research and engineering practices aimed at reducing the risks associated with liquefaction-induced ground damage.

Acknowledgments

The authors express their deep gratitude to the late Professor Dong-soo Kim for his advice on this research. This research received financial support from the National Research Foundation of Korea (NRF) under grant NRF-2022R1A4A503144712 funded by the Korean government (MSIT), as well as from the Korea Ministry of Land, Infrastructure and Transport (MOLIT) through the Innovative Talent Education Program for Smart City.

ORCID

Dong-Hyeong Choi https://orcid.org/0000-0002-6721-9870
Tae-Hyuk Kwon https://orcid.org/0000-0002-1610-8281
Kil-Wan Ko https://orcid.org/0000-0001-5916-4227

References

Adamidis O, Madabhushi GSP (2015) Use of viscous pore fluids in dynamic centrifuge modelling. *International Journal of Physical Modelling in Geotechnics* 15(3),141-149, DOI: 10.1680/jphmg.14.00022

Alarcon-Guzman A, Leonards GA, Chameau JL (1988) Undrained monotonic and cyclic strength of sands. *Journal of Geotechnical Engineering* 114(10):1089-1109, DOI: 10.1061/(ASCE)0733-9410(1988)114:10(1089)

Bertalot D, Brennan AJ, Knappett JA, Muir Wood D, Villalobos FA (2012) Use of centrifuge modelling to improve lessons learned from earthquake case histories. In Eurofuge 2012, Delft, The Netherlands, April 23-24, 2012. Delft University of Technology and Deltares

Bolton MD, Gui MW, Garnier J, Corte JF, Bagge G, Laue J, Renzi R (1999) Centrifuge cone penetration tests in sand. *Géotechnique* 49(4):543-552, DOI: 10.1680/geot.1999.49.4.543

Boulanger RW (2003) High overburden stress effects in liquefaction analyses. *Journal of Geotechnical and Geoenvironmental Engineering* 129(12):1071-1082, DOI: 10.1061/(ASCE)1090-0241(2003)129:12(1071)

Boulanger RW (2003) High overburden stress effects in liquefaction analyses. *Journal of Geotechnical and Geoenvironmental Engineering* 129(12):1071-1082, DOI: 10.1061/(ASCE)1090-0241(2003)129:12(1071)

Boulanger RW, Idriss IM (2014) CPT and SPT based liquefaction triggering procedures. Report No. UCD/CGM.-14, 1

Boulanger RW, Idriss IM (2015) Magnitude scaling factors in liquefaction triggering procedures. *Soil Dynamics and Earthquake Engineering* 79:296-303, DOI: 10.1016/j.soildyn.2015.01.004

Boulanger RW, Idriss IM (2016) CPT-based liquefaction triggering procedure. *Journal of Geotechnical and Geoenvironmental Engineering* 142(2):04015065, DOI: 10.1061/(ASCE)GT.1943-5606.0001388

Carey T, Gavras A, Kutter B, Haigh SK, Madabhushi SPG, Okamura M, Manzari M (2018) A new shared miniature cone penetrometer for centrifuge testing. In: Physical Modelling in Geotechnics, 293-298, CRC Press

Cetin KO, Seed RB, Der Kiureghian A, Tokimatsu K, Harder Jr L F,

Kayen RE, Moss RE (2004) Standard penetration test-based probabilistic and deterministic assessment of seismic soil liquefaction potential. *Journal of Geotechnical and Geoenvironmental Engineering* 130(12): 1314-1340, DOI: 10.1061/(ASCE)1090-0241(2004)130:12(1314)

Cetin KO, Seed RB, Kayen RE, Moss RE, Bilge HT, Ilgac M, Chowdhury K (2018) SPT-based probabilistic and deterministic assessment of seismic soil liquefaction triggering hazard. *Soil Dynamics and Earthquake Engineering* 115:698-709, DOI: 10.1016/j.soildyn.2018.09.012

Dobry R, Abdoun T, Thevanayagam S, El-Ganainy H, Mercado V (2013) Case histories of liquefaction in loose sand fills during the 1989 Loma Prieta Earthquake: Comparison with large scale and centrifuge earthquake tests. Proc., 7th Int. Conf. on Case Histories in Geotechnical Engineering. Missouri University of Science and Technology, Rolla, MO

Dow Chemical Company (2002) Methocel cellulose ethers technical handbook

El-Sekelly W, Dobry R, Abdoun T, Steidl JH (2016) Centrifuge modeling of the effect of preearthquake on the liquefaction resistance of silty sand deposits. *Journal of Geotechnical and Geoenvironmental Engineering* 142(6):04016012, DOI: 10.1061/(ASCE)GT.1943-5606.0001430

Elgamal A, Zeghal M, Taboada V, Dobry R (1996) Analysis of site liquefaction and lateral spreading using centrifuge testing records. *Soils and Foundations* 36(2):111-121, DOI: 10.3208/sandf.36.2_111

Fiegel GL, Kutter BL (1994) Liquefaction mechanism for layered soils. *Journal of Geotechnical Engineering* 120(4):737-755, DOI: 10.1061/(ASCE)0733-9410(1994)120:4(737)

Gui MW, Bolton MD (1998) Geometry and scale effects in CPT and pile design. *Geotechnical Site Characterization* 2:1063-1068

Ha D, Abdoun TH, O'Rourke MJ, Symans MD, O'Rourke TD, Palmer MC, Stewart HE (2010) Earthquake faulting effects on buried pipelines–case history and centrifuge study. *Journal of Earthquake Engineering* 14(5):646-669, DOI: 10.1080/13632460903527955

Hashash YMA, Musgrove MI, Harmon JA, Ilhan O, Xing G, Numanoglu O, Park D (2017) DEEPSOIL 7.0, user manual. University of Illinois at Urbana-Champaign

Hayden CP, Zupan JD, Bray JD, Allmond JD, Kutter BL (2015) Centrifuge tests of adjacent mat-supported buildings affected by liquefaction. *Journal of Geotechnical and Geoenvironmental Engineering* 141(3): 04014118, DOI: 10.1061/(ASCE)GT.1943-5606.0001253

Hughes FE, Madabhushi SPG (2018) The importance of vertical accelerations in liquefied soils. In: Physical Modelling in Geotechnics, 967-973, CRC Press

Hutabarat D, Bray JD (2021) Seismic response characteristics of liquefiable sites with and without sediment ejecta manifestation. *Journal of Geotechnical and Geoenvironmental Engineering* 147(6):04021040, DOI: 10.1061/(ASCE)GT.1943-5606.0002506

Idriss IM, Boulanger RW (2006) Semi-empirical procedures for evaluating liquefaction potential during earthquakes. *Soil Dynamics and Earthquake Engineering* 26(2-4):115-130, DOI: 10.1016/j.soildyn.2004.11.023

Idriss IM, Boulanger RW (2008) Soil liquefaction during earthquakes. California: Earthquake Engineering Research Institute

Ilgaç M (2022) SPT-based probabilistic assessment of seismic soil liquefaction triggering

Inagaki H, Iai S, Sugano T, Yamazaki H, Inatomi T (1996) Performance of caisson type quay walls at Kobe port. *Soils and Foundations* 36: 119-136, DOI: 10.3208/sandf.36.Special_119

Ishihara K, Tatsuoka F, Yasuda S (1975) Undrained deformation and liquefaction of sand under cyclic stresses. *Soils and Foundations* 15(1):29-44, DOI: 10.3208/sandf1972.15.29

Kang S, Kim B, Bae S, Lee H, Kim M (2019) Earthquake-induced ground deformations in the low-seismicity region: A case of the 2017 M5. 4 Pohang, South Korea, earthquake. *Earthquake Spectra* 35(3):1235-1260, DOI: 10.1193/062318EQS160M

Karimi Z, Dashti S, Bullock Z, Porter K, Liel A (2018) Key predictors of structure settlement on liquefiable ground: A numerical parametric study. *Soil Dynamics and Earthquake Engineering* 113:286-308, DOI: 10.1016/j.soildyn.2018.03.001

Kim DS, Kim NR, Choo YW, Cho GC (2013a) A newly developed state-of-the-art geotechnical centrifuge in Korea. *KSCE Journal of Civil Engineering* 17(1):77-84, DOI: 10.1007/s12205-013-1350-5

Kim DS, Lee SH, Choo YW, Perdriat J (2013b) Self-balanced earthquake simulator on centrifuge and dynamic performance verification. *KSCE Journal of Civil Engineering* 17(4):651-661, DOI: 10.1007/s12205-013-1591-3

Korea Meteorological Administration (KMA) (2017) Gyeongju earthquake analysis report (in Korean)

Korea Meteorological Administration (KMA) (2018) Pohang earthquake analysis report (in Korean)

Kostadinov MV, Yamazaki F (2001) Detection of soil liquefaction from strong motion records. *Earthquake Engineering and Structural Dynamics* 30(2):173-193, DOI: 10.1002/1096-9845(200102)30:2<173::AID-EQE3>3.0.CO;2-7

Kramer SL, Sideras SS, Greenfield MW (2016) The timing of liquefaction and its utility in liquefaction hazard evaluation. *Soil Dynamics and Earthquake Engineering* 91:133-146, DOI: 10.1016/j.soildyn.2016.07.025

Lee MG, Ha JG, Cho HI, Sun CG, Kim DS (2021) Improved performance-based seismic coefficient for gravity-type quay walls based on centrifuge test results. *Acta Geotechnica* 16:1187-1204, DOI: 10.1007/s11440-020-01086-5

Liao SS, Whitman RV (1986) Overburden correction factors for SPT in sand. *Journal of Geotechnical Engineering* 112(3):373-377, DOI: 10.1061/(ASCE)0733-9410(1986)112:3(373)

Macedo J, Bray JD (2018) Key trends in liquefaction-induced building settlement. *Journal of Geotechnical and Geoenvironmental Engineering* 144(11):04018076, DOI: 10.1061/(ASCE)GT.1943-5606.0001951

Madabhushi G (2017) Centrifuge modelling for civil engineers. CRC Press

Maurer BW, Green RA, Cubrinovski M, Bradley BA (2014) Evaluation of the liquefaction potential index for assessing liquefaction hazard in Christchurch, New Zealand. *Journal of Geotechnical and Geoenvironmental Engineering* 140(7):04014032, DOI: 10.1061/(ASCE)GT.1943-5606.0001117

Mendoza MJ, Auvinet G (1988) The Mexico earthquake of September 19, 1985—behavior of building foundations in Mexico City. *Earthquake Spectra* 4(4):835-853, DOI: 10.1193/1.1585505

Ministry of Interior Safety (MOIS) (2017) 2016 Gyeongju earthquake white paper (in Korean)

Ministry of Interior Safety (MOIS) (2018) 2017 Pohang earthquake white paper (in Korean)

Ministry of Oceans and Fisheries (MOF) (2018) Pohang port earthquake damage investigation and recovery operation design: Report (in Korean)

Moss RE, Seed RB, Kayen RE, Stewart JP, Der Kiureghian A, Cetin KO (2006) CPT-based probabilistic and deterministic assessment of in situ seismic soil liquefaction potential. *Journal of Geotechnical and Geoenvironmental Engineering* 132(8);1032-1051, DOI: 10.1061/

(ASCE)1090-0241(2006)132:8(1032)
National Disaster Management Research Institute (NDMI) (2019) Development of liquefaction evaluation technique reflecting soil property. Government Publications Registration Number: 11-1741056-00218-13 (in Korean)
Okamura M, Inoue T (2012) Preparation of fully saturated models for liquefaction study. *International Journal of Physical Modelling in Geotechnics* 12(1):39-46, DOI: 10.1680/ijpmg.2012.12.1.39
Özener PT, Greenfield MW, Sideras SS, Kramer SL (2020) Identification of time of liquefaction triggering. *Soil Dynamics and Earthquake Engineering* 128:105895, DOI: 10.1016/j.soildyn.2019.105895
Park SS, Nong Z, Choi SG, Moon HD (2018) Liquefaction resistance of Pohang sand. *Journal of the Korean Geotechnical Society* 34(9):5-17, DOI: 10.7843/kgs.2020.36.9.21
Robertson PK, Wride CE (1998) Evaluating cyclic liquefaction potential using the cone penetration test. *Canadian Geotechnical Journal* 35(3):442-459, DOI: 10.1139/t98-017
Seed HB, Idriss IM (1967) Analysis of soil liquefaction: Niigata earthquake. *Journal of the Soil Mechanics and Foundations Division* 93(3):83-108, DOI: 10.1061/JSFEAQ.0000981
Seed HB, Idriss IM (1971) Simplified procedure for evaluating soil liquefaction potential. *Journal of the Soil Mechanics and Foundations Division* 97(9):1249-1273, DOI: 10.1061/JSFEAQ.0001662
Soga K (1998) Soil liquefaction effects observed in the kobe earthquake of 1995. *Proceedings of the Institution of Civil Engineers-Geotechnical Engineering* 131(1):34-51, DOI: 10.1680/igeng.1998.30004
Stockwell RG, Mansinha L, Lowe RP (1996) Localization of the complex spectrum: The S transform. *IEEE Transactions on Signal Processing* 44(4):998-1001, DOI: 10.1109/78.492555
Suzuki T, Shimizu Y, Nakayama W (1998) Characteristics of strong motion records at the liquefied sites and judgment for liquefaction. 11th European Conference on Earthquake Engineering. Rotterdam: Balkema
Takada S, Ozaki R (1997) A judgment for liquefaction based on strong ground motion. Proceedings of 24th JSCE Earthquake Engineering Symposium, Kobe, 24-26 July. JSCE; 261-264 (in Japanese)
Tiznado JC, Dashti S, Ledezma C, Wham BP, Badanagki M (2020) Performance of embankments on liquefiable soils improved with dense granular columns: Observations from case histories and centrifuge experiments. *Journal of Geotechnical and Geoenvironmental Engineering* 146(9):04020073, DOI: 10.1061/(ASCE)GT.1943-5606.0002309
Tsuchida H (1970) Prediction and countermeasure against the liquefaction in sand deposits. Abstract of the seminar in the Port and Harbor Research Institute, 31-333
van Ballegooy S, Green RA, Lees J, Wentz F, Maurer BW (2015a) Assessment of various CPT based liquefaction severity index frameworks relative to the Ishihara (1985) H1–H2 boundary curves. *Soil Dynamics and Earthquake Engineering* 79:347-364, DOI: 10.1016/j.soildyn.2015.08.015
van Ballegooy S, Wentz F, Boulanger RW (2015b) Evaluation of CPT-based liquefaction procedures at regional scale. *Soil Dynamics and Earthquake Engineering* 79:315-334, DOI: 10.1016/j.soildyn.2015.09.016
Wang X (2021) Empirical probability distribution models for soil-layer thicknesses of liquefiable ground. *Journal of Geotechnical and Geoenvironmental Engineering* 147(6):06021005, DOI: 10.1061/(ASCE)GT.1943-5606.0002537
Yamamoto M, Nozu S, Miyajima M, Kitaura M (1999) Proposal for liquefaction indices and their verification. Proceedings of 25th JSCE Earthquake Engineering Symposium, Tokyo, 29-31 July. JSCE; 417-420 (in Japanese)
Yoshimi Y, Tanaka K, Tokimatsu K (1989) Liquefaction resistance of a partially saturated sand. *Soils and Foundations* 29(3):157-162, DOI: 10.3208/sandf1972.29.3_157
Youd TL, Bartlett SF (1991) Case histories of lateral spreads from the 1964 Alaska earthquake. Proc. 3 Japan/US workshop on Earthquake Resistrant Design of Lifeline Facilities and Countermeasures for Soil Liquefaction. Nat. Cent. for Earthquake Engineering Research, Tech. Rep. NCEER-91, 175-189
Youd TL, Idriss IM (2001) Liquefaction resistance of soils: summary report from the 1996 NCEER and 1998 NCEER/NSF workshops on evaluation of liquefaction resistance of soils. *Journal of Geotechnical and Geoenvironmental Engineering* 127(4):297-313, DOI: 10.1061/(ASCE)1090-0241(2001)127:4(297)
Zeghal M, Elgamal AW (1993) Lotung site: Downhole seismic data analysis. Palo Alto: Electric Power Research Institute
Zeghal M, Elgamal AW, Tang HT, Stepp JC (1995) Lotung downhole array. II: Evaluation of soil nonlinear properties. *Journal of Geotechnical Engineering* 121(4):363-378, DOI: 10.1061/(ASCE)0733-9410(1995)121:4(363)
Zeghal M, Goswami N, Kutter BL, Manzari MT, Abdoun T, Arduino P, Ziotopoulou K (2018) Stress-strain response of the LEAP-2015 centrifuge tests and numerical predictions. *Soil Dynamics and Earthquake Engineering* 113:804-818, DOI: 10.1016/j.soildyn.2017.10.014